Title
Uniform, Large-Area, Highly Ordered Peptoid Monolayer and Bilayer Films for Sensing Applications

Authors
Murray, Daniel J
Kim, Jae Hong
Grzincic, Elissa M
et al.

Uniform, Large-Area, Highly-Ordered Peptoid Monolayer and Bilayer Films for Sensing Applications

Daniel J. Murray[†1], Jae Hong Kim,[†1] Elissa M. Grzincic,[1] Samuel C. Kim,[2] Adam R. Abate,[2,3] Ronald N. Zuckermann*[1]

[1]The Molecular Foundry, Lawrence Berkeley National Laboratory, 1 Cyclotron Road, Berkeley, California 94720, USA.
[2]Department of Bioengineering and Therapeutic Sciences, University of California, San Francisco, California, 94158 USA
[3]Chan Zuckerberg Biohub, San Francisco, California, USA.

Abstract

The production of atomically defined, uniform, large area 2D materials remains as a challenge in materials chemistry. Many methods to produce 2D nanomaterials suffer from limited lateral film dimensions, lack of film uniformity, or limited chemical diversity. These issues have hindered the application of these materials to sensing applications, which require large area uniform films to achieve reliable and consistent signals. Furthermore, the development of a 2D material system that is biocompatible and readily chemically tunable has been a fundamental challenge. Here we report a simple, robust method for the production of large area, uniform, and highly tunable monolayer and bilayer films from sequence-defined peptoid polymers, and their application as highly selective molecular recognition elements in sensor production. Monolayers and bilayer films were produced on the centimeter scale using Langmuir-Blodgett methods, and exhibited a high degree of uniformity and ordering as evidenced by atomic force microscopy, electron diffraction and grazing incidence X-ray scattering. We further demonstrated the utility of these films in sensing applications by employing the bio-layer interferometry technique to detect the specific binding of the pathogen derived proteins, shiga toxin and anthrax protective antigen, to peptoid-coated sensors.
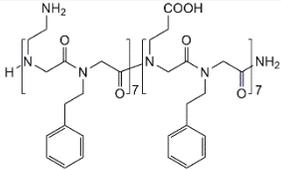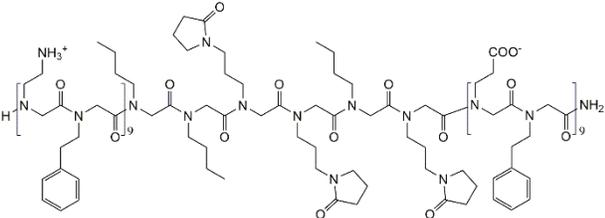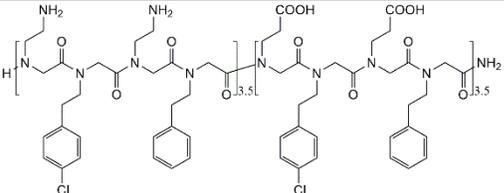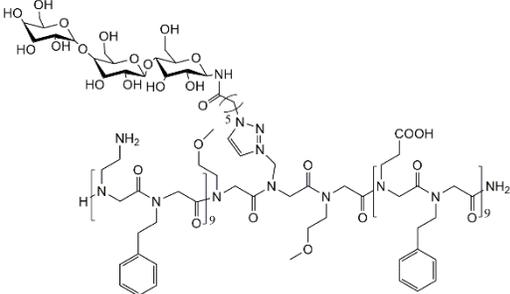
2

Introduction

Two-dimensional (2D) nanomaterials such as graphene and metal chalcogenides have had gained enormous interest due to their promising structural, optical, electronic, and mechanical properties.[1,2] Inspired by the huge opportunities of these materials in a variety of applications, organic analogs of these 2D nanomaterials have recently been investigated by many groups.[3-5] Notably, the use of polymer building blocks to construct 2D materials through a self-assembly approach has enabled high chemical tunability and biocompatibility to be achieved.[6,7] One of the most attractive building blocks are peptoid polymers, bio-inspired oligomers of sequence-defined *N*-substituted glycines. One key feature of peptoids is the incredible diversity of side-chain residues that can be incorporated on its backbone. Additionally, precise control of chain length and monomer sequence can be achieved through the solid-phase submonomer method.[8] The lack of chirality and hydrogen bond donors in the peptoid backbone enables the interactions between polymer chains to be programmed through side chain selection.[9] This provides a means to design and control the self-assembly process of these polymers, and results in the ability to create supramolecular peptoid assemblies with atomically-defined structural features and high crystallinity.[10-15] Adopting these unique properties, amphiphilic diblock peptoid polymers have been synthesized which assemble into atomically-defined 2D nanomaterials with uniform thickness (~ 2.7 nm) and high area/thickness ratio (> 10^9 nm^{-1}) at the air-water or oil-water interface.[16-19] Furthermore, molecular engineering of these nanosheets[18] by chemical tailoring of the peptoid strands to integrate molecular recognition elements creates a robust platform that is ideally suited for biomedical applications such as biosensing and the remediation of threat agents. Nevertheless, in order to successfully scale production of these materials to an industrial scale and create practical devices, there still remain significant challenges in fabrication. The key steps requires simultaneous control over several length scales. Sensing devices, for example, could require the preparation of homogeneous peptoid monolayer or bilayer films up to the centimeter scale. Therapeutic applications would likely require production of uniformly-sized peptoid nanosheets on the micron scale.
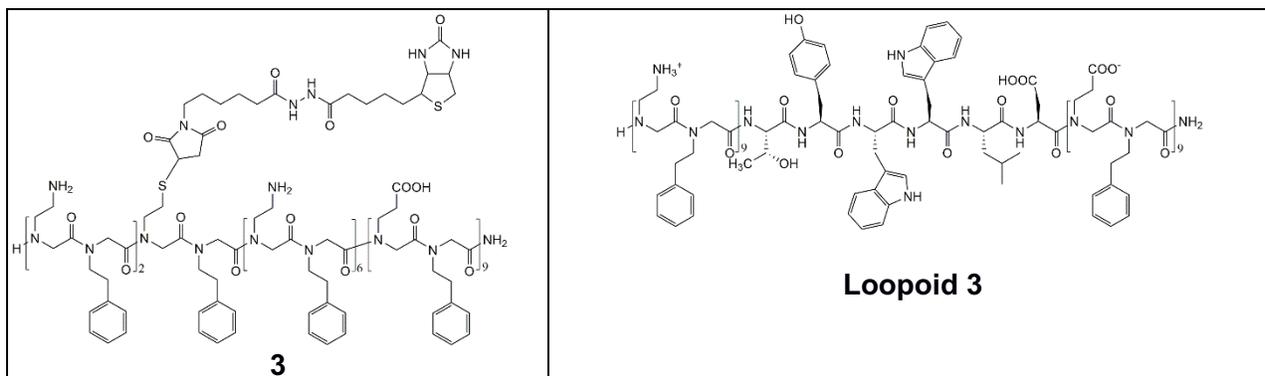
3

This work addresses these challenges and demonstrates the utility of peptoid monolayers and bilayers films in molecular recognition by employing the surface-based platform of bio-layer interferometry (BLI). The technique of BLI has attracted a great deal of interest as a real-time, label-free, high-throughput, and high sensitivity bio-sensing technique.[20] This method is based on the measurement of optical interference patterns generated by white light reflected off a functional surface and that of an internal reference surface. As analytes bind to the functional surface a shift in the interference pattern is can be measured and related back to specific binding interactions. In order to obtain specific and sensitive response for targets, it requires the functional surface to be modified by the conjugation of functional chemical or biomolecular recognition elements. Although several strategies for the conjugation of functional biocomponents on a desired substrate have been developed,[21] there remain shortcomings, such as uncontrolled display density and molecular orientation. This can result in a loss of binding activity and an increase of background signal.[22] The deposition of functionalized peptoid monolayers integrating molecular recognition elements onto a BLI sensor may mitigate these issues, and provide a highly tunable platform. Using this method, molecular recognition elements incorporated as a "loop domain" insert in the middle of a peptoid sequence can be displayed on a hydrophilic and zwitterionic nanosheet surface that helps prevent non-specific binding.[18,23] Furthermore, peptoids with loop domains or "loopoids" are versatile tools for the chemical conjugation and display of functional ligands through the addition of desired amine monomers in the loop domain. For instance, alkyne-containing loopoid nanosheets were conjugated with azide-functionalized carbohydrates *via* click chemistry, and were shown to have high and specific binding affinity for target proteins owing to the multivalency originating from the high display density of carbohydrates on the nanosheet surface.[24]

Herein, we report the fabrication of large-area and uniform peptoid nanofilms on silicon and glass substrates based on Langmuir-Blodgett techniques. A peptoid monolayer film was prepared at the air-water interface in a Langmuir trough, then, successfully deposited on the substrate by the Langmuir

Blodgett (LB) method. Peptoid bilayer films were also assembled by the deposition of second monolayer onto the hydrophobic face of a monolayer nanofilm by the Langmuir Schaefer (LS) method. The uniformity, high ordering, large-area of prepared peptoid nanofilm was demonstrated by a combination of optical microscopy, atomic-force microscopy, electron microscopy, and X-ray diffractometry. Importantly this coating method is applicable to a wide variety of peptoid sequences, making the functionality of the resulting films easily tunable. Using these methods, we also show that the peptoid films can be used to make peptoid nanosheets with uniform shape and size through a photolithography-based approach using a series of functionalized peptoids (Table1). Additionally, loop-functionalized peptoid monolayers were coated onto the tip of optical fibers, and used as a BLI biosensing platform. Based on the structural properties of the resultant multivalent peptoid nanofilms, we confirmed significant improvement of BLI signal against multimeric toxin-related proteins, such as shiga toxin 1 subunit B (STX 1B) and anthrax protective antigen $[(PA63)_7]$, through a multivalent manner.

Table 1. Peptoids used in this study to prepare monolayer and bilayer-coated surfaces.

Linear Peptoids	Loop Inserted Peptoids
1	**Loopoid 1**
2	**Loopoid 2**

3

Loopoid 3

Results and Discussion

Peptoid Monolayer Preparation and Deposition by LB Technique

The scale-up of free-floating nanosheets in aqueous solution has been previously achieved by a vial-rocking method,[15] which allows repeated lateral surface compressions to be applied to a key assembly intermediate, a spontaneously forming monolayer at the air-water or oil-water interface.[25] Although this method provides multi-milligram quantities of nanosheets, they are small in size (<1 mm) and have a broad distribution of shape and size. This hinders application of these materials for sensing applications which require a uniform coating of material, often over a large area. To address this problem, we employed the LB technique to prepare large (centimeter scale) and uniform peptoid monolayers and subsequently bilayers at the air-water interface in a Langmuir trough (Figure 1).
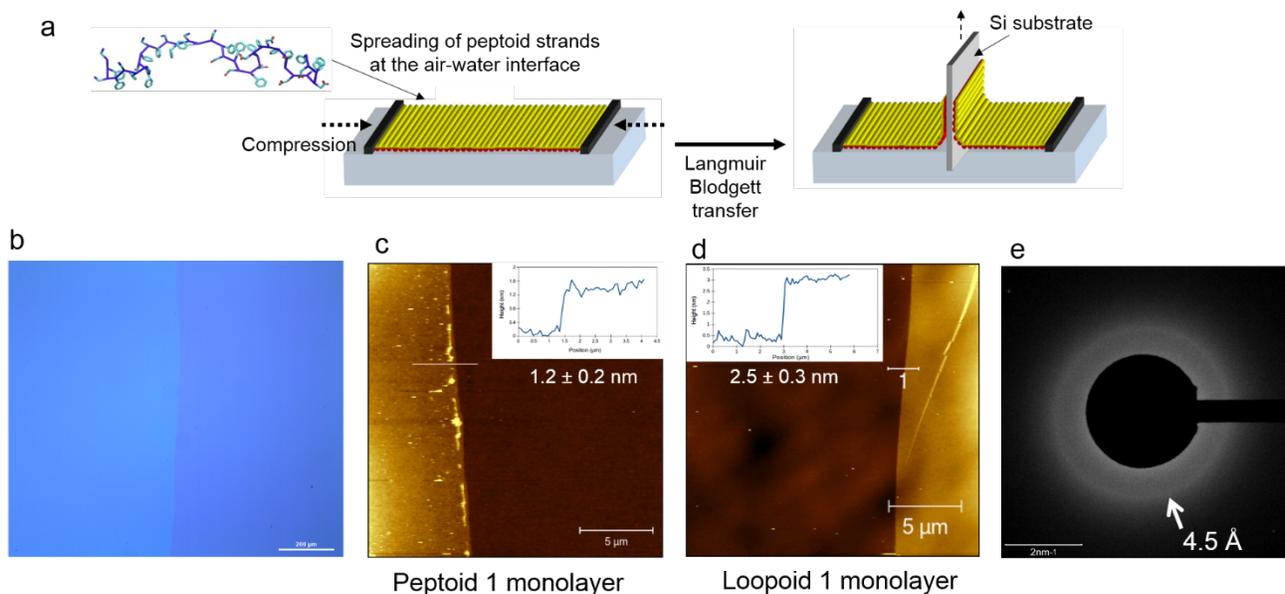
Figure 1. (a) Schematic illustration of fabrication of peptoid monolayer film by Langmuir Blodgett transfer method. (b) Reflectance optical image of B28 monolayer on Si/SiO₂. The coated portion appears a lighter blue on the left and the uncoated portion is darker blue on the right. (c and d) AFM images of peptoid **1** and loop-inserted (**loopoid 1**) monolayer film. (d) SAED pattern of peptoid **1** monolayer film.

A major disadvantage of this method is the requirement of large subphase volumes (~100 mL or more) which cause an enormous consumption of peptoid stock if the standard method of peptoid adsorption from bulk solution is utilized for monolayer formation.[15] In order to alleviate this problem, we directly spread a small volume of peptoid from a concentrated stock solution onto the air-water interface. Specifically, 10 μL of peptoid **1** stock solution (2 mM in 1:1 water:DSMO) was applied to the surface of 100 mL subphase (2 mM Tris buffer, pH 8.0) in a Langmuir trough. We use this amount of peptoid to provide a slight excess of molecules relative to the amount required to form exactly one monolayer. This accounts for some loss to the bulk and provides a small reservoir of molecules to allow for the monolayer equilibration process. The DMSO in the stock solution is used to prevent self-assembly in the stock solution and dissolves into the subphase upon spreading. Upon the spreading of **1**, the surface pressure rapidly increased to ~16 mN m⁻¹ due to immediate spreading of peptoid strands at the interface (Supplemental Figure S1). After this initial spreading the surface pressure began to gradually decrease, indicating that desorption of peptoids is faster than adsorption at this stage. After a period of about 2 min,

the surface pressure leveled out and a gradual rise of surface pressure was observed, indicating that adsorption of peptoid strands to the interface eventually dominates. This surface pressure increase eventually stabilized to reach an equilibrium state at ~22 mN m^{-1}. When this equilibrium state was reached the film was compressed to 30 mN m^{-1}, just below the collapse pressure, to form the compressed peptoid monolayer at the interface. On our trough this resulted in a monolayer size of 82 cm^2. Details of the peptoid monolayer formation and collapse of this peptoid has studied in detail.[26]

We next transferred the peptoid monolayer onto the surface of hydrophilic or hydrophobic substrates. For a hydrophilic substrate, monolayers of **1** were transferred on the surface of plasma cleaned Si/SiO$_2$. The transfer of **1** monolayer was accomplished by the immersion of the substrate into the subphase before spreading peptoids on the interface, and withdrawing the substrate at a rate of 1 mm/min through the interface after peptoid monolayer formation. As the monolayer was transferred off the air/water interface, the surface pressure was held constant at 30 mN m^{-1}, and a decrease in the trough surface area was observed. This decrease in area was consistent with the area of the substrate, giving a transfer ratio close to 1 which indicates that peptoid monolayer was uniformly coated on the surface of substrate. Transfer of the monolayer at the equilibrium spreading pressure of 22 mN m-1 resulted in lower transfer ratios and thus, a less uniform coating. The Si/SiO$_2$ substrate allows observation of the deposition of **1** monolayer by reflectance optical microscopy (Figure 1b). We found that **1** monolayer was extensively covered on the substrate without observable defects. Moreover, the contrast homogeneity suggested that **1** monolayer had a uniform thickness. Based on the height measurement by atomic force microscopy (AFM), the thickness was approximately 1.2 ± 0.2 nm, which is consistent with the expected height of the peptoid strands that are laying with the backbone parallel to the substrate (Figure 1c).

We also confirmed that peptoid monolayer could be coated on to hydrophobic substrate using a 2-phenylethyl-functionalized Si/SiO$_2$ substrate. This substrate was lowered down through the

compressed monolayer at 1 mm/min and then removed after the subphase had been aspirated clean. Optical imaging showed that monolayers transferred in this fashion are uniformly coated without observable defects just as seen for transfer to hydrophilic Si/SiO₂ (Supplementary Figure S2). Static contact angle measurements of this monolayer showed a water contact angle of 34°, in contrast to 86° for the bare phenethyl modified Si/SiO₂. These contact angles where observed to be stable, indicating the films were not delaminating from the substrate. This shows that monolayers can be coated with either the hydrophilic side or the hydrophobic side exposed. The ability to transfer the monolayer with the hydrophilic side exposed will enable the creation of surfaces coated with surface-functionalized peptoid monolayers for aqueous analyte binding applications.

We further demonstrated that this method of monolayer formation and transfer was applicable to other peptoid sequences. An AFM image of a monolayer from a loop inserted peptoid, **loopoid 1**, that was transferred to a phenethyl modified Si/SiO₂ surface, is shown in Figure 1d. The measured thickness of the monolayer was 2.5 ± 0.3 nm. This thickness is indicative of a monolayer that has the loop domains protruding from the surface.[18] Transfer to the hydrophobic surface results in the loop domains being exposed on the substrate surface. The ability the coat surfaces in this way leads to the possibility of fabricating surfaces with a large area uniform coating of monolayers bearing molecular recognition elements.

To investigate the internal ordering to the monolayer we performed selected area electron diffraction (SAED). The monolayers were transferred to plasma treated ultra-thin carbon TEM grids, by pulling them up through the monolayer as described above. Diffraction was performed at 77K in order to reduce beam damage. The patterns show an isotropic peak at 1.4 Å⁻¹ which corresponds to a 4.5 Å spacing (Figure 1e). Diffraction at 4.5 Å in peptoid nanosheets has previously been shown to result from the spacing between aligned peptoid chains.[13]

Peptoid Bilayer Formation by Langmuir-Schaefer Technique

Since the LB deposition of the hydrophilic face of a peptoid monolayer on hydrophilic Si/SiO$_2$ substrate results in the exposure of a uniform layer of hydrophobic 2-phenylethyl groups, we sought to use the Langmuir-Schaefer (LS) method for transferring a second peptoid monolayer in an LB trough to fabricate the peptoid bilayer structure (Figure 2a) that has previously been reported in peptoid nanosheets.[13] This seeks to provide a large area and uniform peptoid bilayer film that is not achievable using the current vial-rocking method.[15] Before the deposition of the second peptoid monolayer, the first peptoid monolayer film was dried under vacuum at 50 °C for 2 hr to remove any remaining aqueous solution between the monolayer and substrate to ensure adhesion. Subsequently, the LS deposition method was applied to deposit a second peptoid monolayer. A transfer ratio could not be calculated since the subphase was aspirated clean before removal of the substrate. Reflectance optical microscope images of the prepared film showed that it was homogeneously deposited across the substrate (Figure 2b). The edges of the peptoid bilayer film have delaminated and folded back over on the substrate, indicating that the resulting film has the mechanical strength necessary to remain intact once it has been removed from the support substrate (Figure 2c). The thickness of the bilayers was shown to be 3.0 ± 0.2 nm by AFM (Figure 2d). This is consistent with previously reported bilayer nanosheets. Moreover, the bilayer has a surface roughness similar to the underlying SiO$_2$. This points to a uniform packing of peptoids within the film.
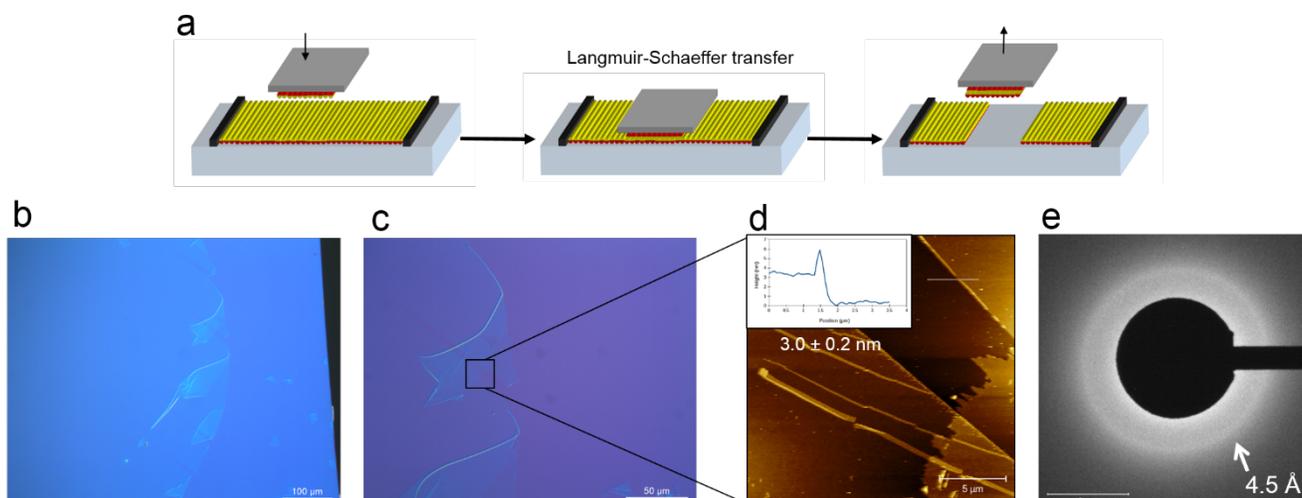
Figure 2. (a) Schematic illustration of peptoid bilayer film by Langmuir Schaeffer transfer method. (b, c) Reflectance optical microscopic images of peptoid **1** bilayer film on Si/SiO$_2$. (d) AFM images and height profile of peptoid **1** bilayer film. (e) SAED pattern of peptoid **1** bilayer film.

Staining the bilayer film with Nile red, known to stain nanosheets in solution, and imaging by fluorescence microscopy reveals a direct correlation of emission with reflectance optical microscopy images (Supplementary Figure S3). This gives further evidence for bilayer formation, as Nile red has been shown to selectively incorporate into the hydrophobic core of bilayer nanosheets.[13] Staining of the monolayer films results in no fluorescence emission.

We further investigated the internal ordering of monolayers and bilayers of peptoid **1** using grazing-incidence wide-angle X-ray scattering (GIWAXS) and selected area electron diffraction (SAED) by transmission electron microscopy (TEM). In the GIWAXS patterns (Supplementary Figure S4) both monolayer and bilayer on Si(100) have an in-plane peak at 1.37 Å^{-1} corresponding to a 4.6 Å spacing which is not seen in the out-of-plane direction. The higher intensity of this peak for the bilayer is consistent with having an additional layer present. This spacing is indicative of the chain to chain spacing of parallel polymers that has previously reported in floating peptoid monolayers.[25] By comparing this data to diffraction from peptoid monolayers at the air-water interface,[25] we can conclude that the chain alignment is preserved during the LB transfer process. The absence of this peak in the out of plane

direction indicates alignment of the peptoid chains in the plane of the substrate, which is also consistent with AFM height measurements discussed previously. Additionally, a peak corresponding to the interlayer spacing of monolayers is seen at 0.41 A^{-1} with the second and third harmonic seen at 0.83 A^{-1}, and 1.26 A^{-1} in the out-of-plane direction for the bilayer (Supplementary Figure S4). This set of peaks is absent in the pattern for the monolayer.

Analysis of the bilayer films by selected area electron diffraction (SAED) was also performed. Just as for the monolayers, we performed the diffraction experiments at 77 K to minimize beam damage to the films. Diffraction patterns of bilayers of **1** (Figure 2e) show an isotropic peak at 1.4 $Å^{-1}$ corresponding to a 4.5 Å spacing just as seen in the monolayer films. This is consistent with the above GIWAXS data and shows the films consist of aligned peptoid chains laying in the plane of the substrate they were transferred to.

Monolayer and Bilayer annealing

To date all of the reported diffraction data on films of peptoid **1** has shown an isotropic peak at 1.4 $Å^{-1}$ which has been shown to result from the alignment of the peptoid backbones. Since this peak is anisotropic we know that the domain size of the aligned peptoid chains is much smaller than the spot size in the SAED experiments. In turn, this shows that the monolayer and bilayer films have little to no long-range ordering. We next investigated if the long-range ordering of the films could be improved using thermal anealling. Because the chain ordering is known to occur during the monolayer formation step,[25] we used an annealing process in which the monolayer was annealed at 50 °C for 3 hr while being compressed to 30 mN/m at the air water interface. After the 3 hr annealing the monolayer was transferred off the interface as previously described. SAED over an area of about 0.75 μm^2 at 77 K of this annealed monolayer shows a set of sharp spots at 1.4 $Å^{-1}$ in contrast to the diffraction ring seen in the unannealed monolayer (Figure 3a). This spot disappears after prolonged exposure to electron doses of ~10 $e^-/Å^2$.

The dramatic increase of long-range order in the monolayer, as indicated by the diffraction spots, led us to prepare bilayers using this method. For this we used the LS method with two annealed monolayers. The SAED patterns for the annealed bilayers show a set of spots at 1.4 Å^{-1} as well, however, there is now an additional set at 1.4 Å^{-1} that is oriented in a different direction (Figure 3b). This second set is weaker in intensity indicating that most of the peptoid alignment is in the direction of the more intense spot. This demonstrates the importance of thermal annealing at the monolayer stage to create long-range order in the subsequent films.
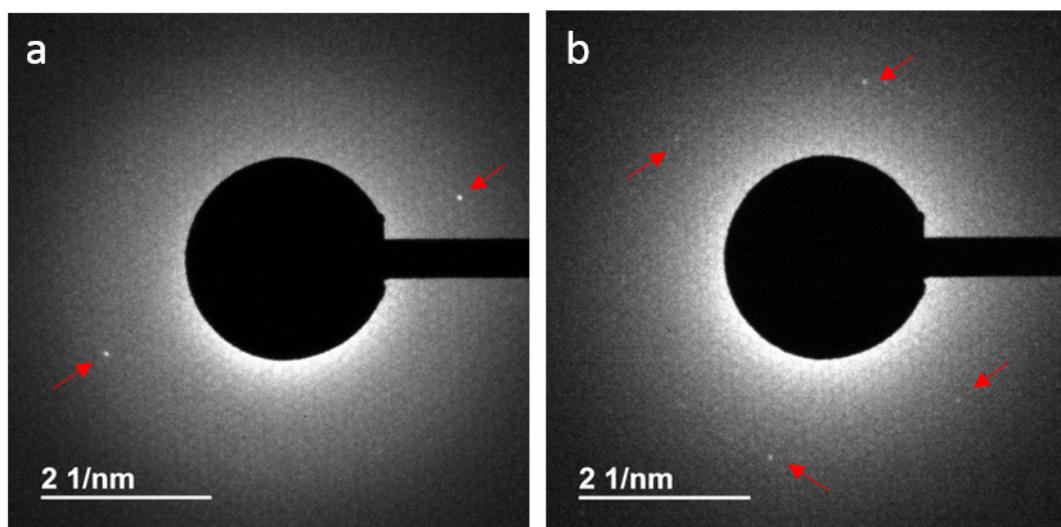

Figure 3. SAED patterns of thermally annealed peptoid **1** monolayer (a) and bilayer (b).

Photopatterning of Peptoid Nanosheets for Size and Shape Uniformity

By taking advantage of a method previously described by our group[27] for the production of covalently crosslinked nanosheets, we show that bilayer films can be photo-patterned to control their lateral dimensions. Patterning of these films should enable the production of bilayer peptoid structures of defined size and shape. The general method for photopatterned film production is shown in Figure 4a. First, bilayer films of peptoid **2** were deposited on Si/SiO$_2$. Optical microscopy (Supplemental Figure S5) showed that these films behave similar to peptoid **1**. Some delamination was observed along the

edges of the substrate, but the bulk of the substrate was covered with a continuous film. AFM imaging (Supplemental Figure S5) showed that this film is slightly thicker than peptoid **1**. This is consistent with previous reports of nanosheets made in solution.
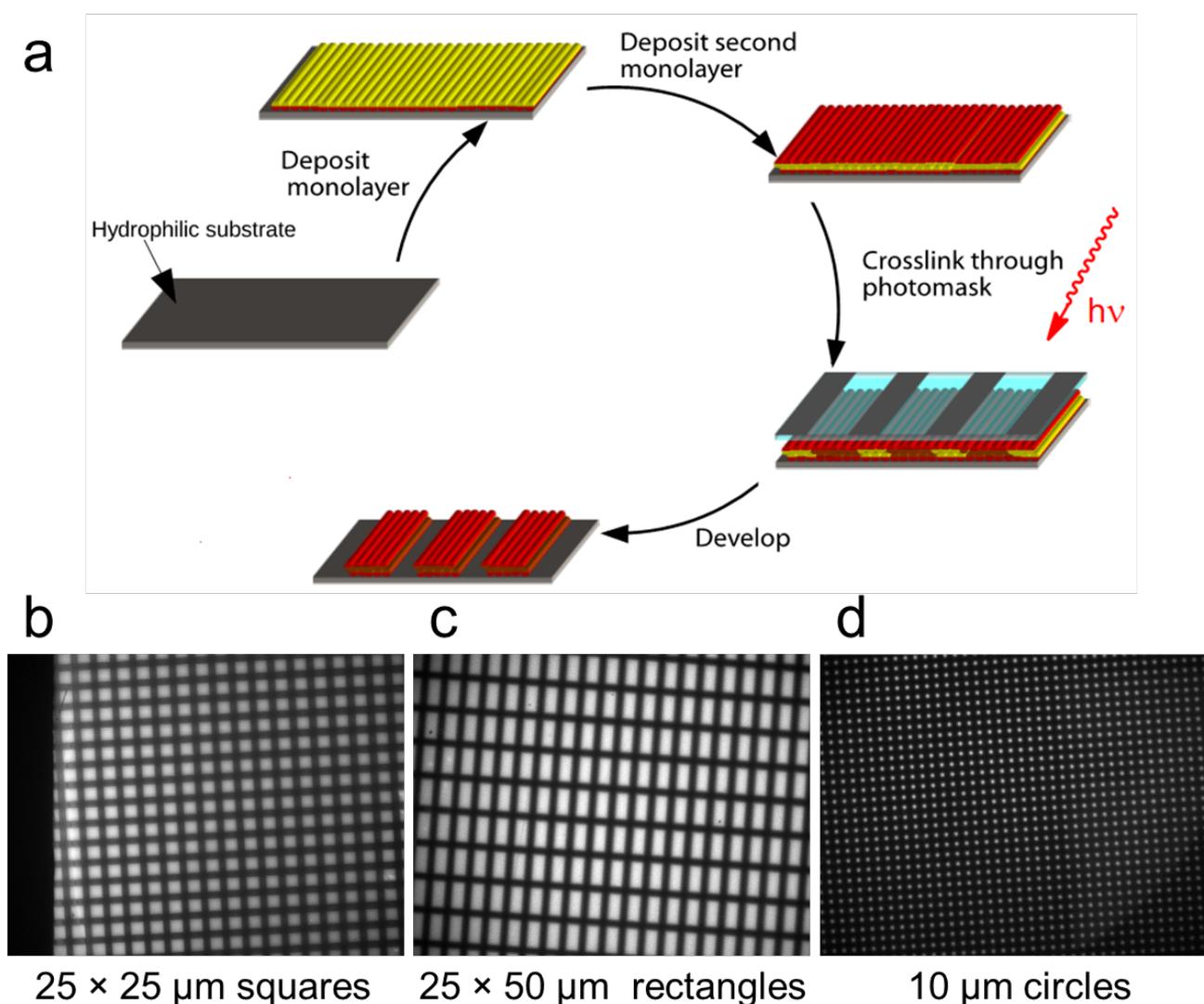
Figure 4. (a) Schematic illustration of photopatterning of peptoid bilayer film by UV cross-linking method. The use of photo-reactive peptoid **2** allows bilayers to be deposited and then crosslinked with the desired pattern. (b, c, and d) Fluorescent microscopic images of peptoid nanosheets with uniform shape such as squares, rectangles, and circles.

Following bilayer film production, the films were irradiated through a photomask with 254 nm light to photo-crosslink in the hydrophobic core. The crosslinking renders the film insoluble in organic solvents, allowing the un-irradiated portion of the film to be removed by washing with ethanol. Finally,

the developed films were stained with Nile red and imaged with fluorescence microscopy (Figure 3b-d). We demonstrated this technique to produce three different shapes (squares, rectangles, circles) but the size and shape is purely a function of the photomask and can be tailored to the desired application.

Loop-Functionalized Peptoid Monolayer as Bio-Layer Interferometric Sensing Platform

Because of the large-area and uniformity of peptoid monolayer and bilayer using our developed method, it can be useful for the precise surface display of molecular recognition elements (e.g., peptides, peptoids, drugs, carbohydrates, etc.). We applied our method for the deposition of functionalized loopoid monolayers to the tip of glass optical fibers to detect analytes using BLI technique as shown in Figure 5a. For the deposition of the loopoid monolayer, we first cleaned the surface of optical fiber by immersion into 0.01 M NaOH for 1 hour, then, aromatic groups were attached to the surface by the reaction with 2-phenylethylsilane vapor overnight. Using the resultant hydrophobic surface of the optical fiber, we introduced the loopoid monolayer by Langmuir-Schaefer deposition as described above. To demonstrate that the monolayer deposition occurred with the proper solution display of ligands, we first introduced a biotin-conjugated peptoid **3** monolayer, and then observed the binding of Alexa Fluor 647 conjugated streptavidin by fluorescent microscopy. We confirmed the binding activity of biotin groups on the surface by the resultant increase of Alexa Fluor 647's fluorescence within biotin-B36 monolayer (Supplemental Figure S7). For the generation of interferometric signal against interested targets as shown in Figure 5b, we employed globotriose-conjugated **loopoid 2** and peptide 6mer (TYWWLD)-inserted **loopoid 3** which are well-known functional ligands as binders for toxin-related proteins, such as shiga toxin subunit 1B (Stx) and anthrax protective antigen $(PA63)_7$, respectively.[28,29] We also used plain peptoid strands and lactose-conjugated **loopoid 4** as negative controls. Upon Stx binding to the monolayer of **loopoid 2**, the interferometric signal increased and decreased in accordance with association and dissociation phase (Figure 5c). In addition, there was no binding to loopless control monolayers from peptoid **1** and lactose-

conjugated monolayers from **loopoid 3**. These results indicate that globotriose moiety of **loopoid 2** monolayers were adequately exposed on the surface of optical fiber, while maintaining their binding activity and preventing non-specific binding. We also observed that selective response against $(PA63)_7$ only appeared in case of **loopoid 3**. Therefore, large area and uniform loopoid monolayer is suitable for the surface modification of optical fiber and the label-free real-time measurement of target binding by the BLI technique.
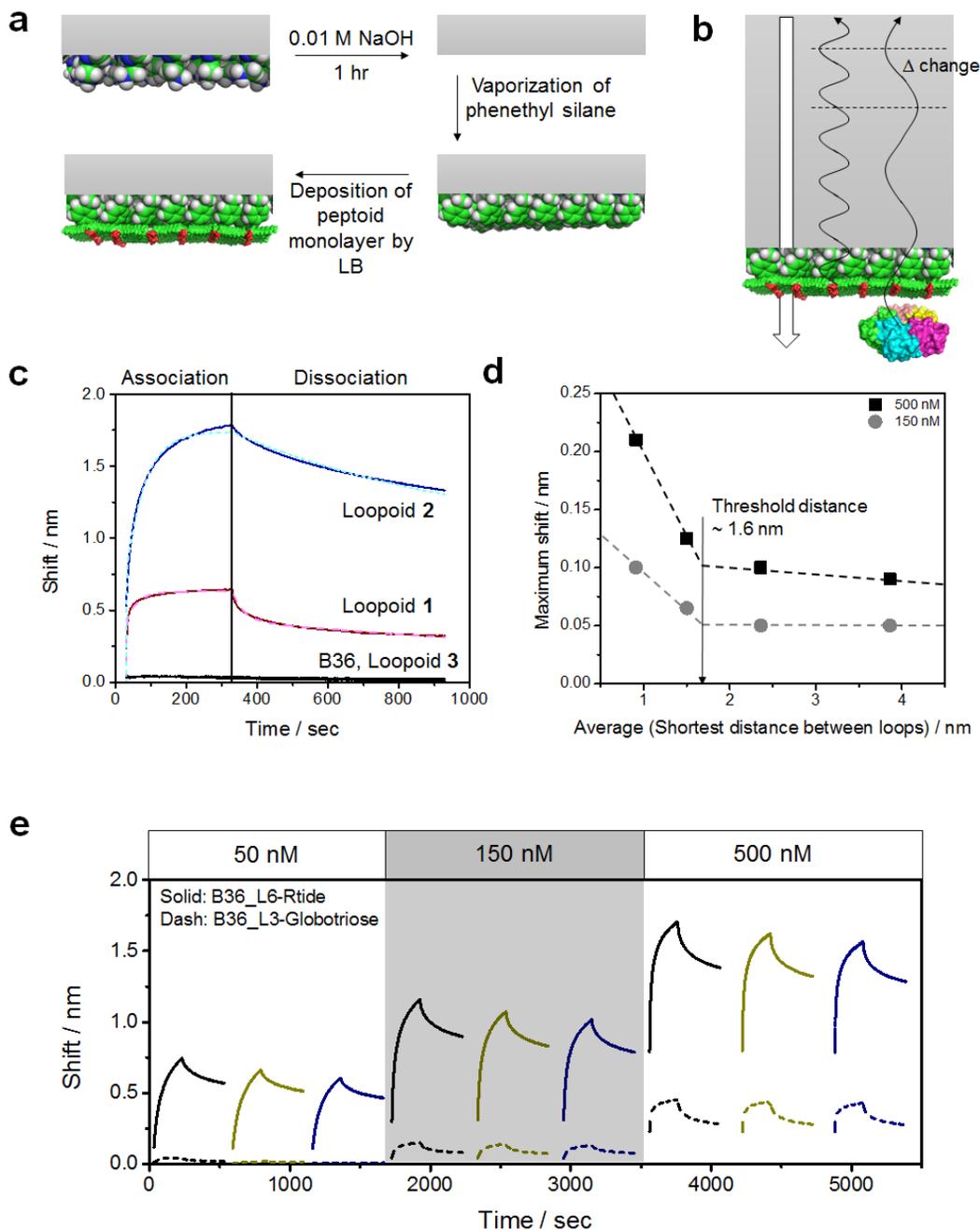
Figure 5. Biosensing platform based on loop-functionalized peptoid monolayer-coated optical fiber by interferometry. (a) Scheme for the surface modification of an optical fiber by the LB technique to deposit a large and uniform peptoid monolayer. (b) Schematic illustration of the peptoid monolayer-deposited optical fiber for the detection of protein binding by interferometry. (c) Binding (solid) and fitting (dashed) curve of **loopoid 1** monolayer against 500 nM STX 1B, **loopoid 2** monolayer against 500 nM (PA63)$_7$ (red and pink), and negative control sample (e.g., peptoid **1** and **loopoid 3** monolayers) against 500 nM (PA63)$_7$ and Stx 1B (black). (d) Plot of maximum intensity of wavelength shift against the average of shortest distance between loops. The shortest distance between loops were adapted from the literature[20] (e) Demonstration of the regeneration and reusability of **loopoid 1** and **loopoid 2** coated sensor tips. Sensor tips were immersed into 10 mM HCl solution during 10 sec at room temperature, then, neutralized by using PBS buffer containing 0.1% tween 20 during 10 sec.

Based on the BLI response curves, we studied binding parameters (e.g. association/dissociation rate and binding constant) of monolayers of **loopoid 2** and **loopoid 3** against Stx 1B and $(PA63)_7$. Using a two-to-one heterogeneous ligand model, the binding constant (K_D) of the loopoid **2** and loopoid **3** monolayers was determined to be approximately 15.5 and 31.1 nM, respectively. By contrast, the K_D of univalent globotriose and half-maximal inhibitory constant (IC_{50}) of TYWWLD for Stx 1B and $(PA63)_7$ are known to be considerably weaker, at 2 mM and 150 μM, respectively.[30,31] The enhanced binding affinity from the millimolar or micromolar range to the nanomolar range, suggests that the surface displayed ligands on the loopoid monolayer interact with their target proteins in a multivalent manner.[31] In addition, Battigelli *et al*. recently reported the enhancement of binding affinity to sugar-functionalized nanosheets through multivalent interactions with lectins, and that the binding was dependent upon the ligand display density.[24] Thus, we examined the relationship between the binding affinity and ligand display density using a series of monolayers prepared by dilution of **loopoid 2** with peptoid **1**. We found a dramatic increase of signal against Stx 1B binding when the globotriose units are less than 1.6 nm apart (on average) from each other. This threshold distance is well accordance with the shortest distance between binding sites on Stx 1B (~1.4 nm as shown in Supplemental Figure S8), showing that the accumulation of globotriose on peptoid nanosheets induced cooperative binding behavior of multiple carbohydrates. Thus, the multivalency from the molecular structure of the loopoid monolayer can improve the sensitivity for multivalent targets.

We further studied the reusability of BLI sensor tips made from **loopoid 2** and **loopoid 3** by stripping of bound proteins by the immersion of sensor tips into 10 mM HCl solution during 10 sec at room temperature. The binding efficiency was well maintained for three cycle at each different concentration of proteins (Figure 5e), hence indicating a good reusable capability of loopoid monolayers for BLI-based biosensing platform. We also tested the stability of these loopoid monolayer coated tips by the measurement of the binding activity using stored loopoid monolayer in 10 mM Tris buffer (pH

8.0) for 9 days at 4 °C. We obtained a similar binding signal and K_D (~20 nM) with the stored sample as to the fresh sample (Supplemental Figure S9). Taken together, large area and uniform loopoid monolayer deposition can be a versatile tool for the surface modification of the BLI sensor format to detect bio-analytes with high sensitivity and reliability.

Conclusion

Herein, we demonstrated the fabrication large area peptoid monolayer and bilayer films with long-range order using Langmuir techniques. These methods have been shown to result in films that are highly uniform as shown by optical microscopy and AFM. The internal ordering of the films was investigated by SAED and GIWAXS and reviled that the transferred films consist of aligned peptoid strands that lay in the plane of the substrate. This structure is locally similar to that reported previously for the large-scale preparation of free-floating nanosheets in solution, but with irregular shapes and sizes. Films can be fabricated from a wide variety of peptoids that display surface features at controllable densities, that can be used as molecular recognition elements for sensing. As such, we have shown that by coating sensors with monolayers of loopoids for use in BLI that we can fabricate highly sensitive, selective, and robust platform from detection of select targets. The wide applicability of the film fabrication methods to peptoids of very diverse chemical functionalities results in the ability to tune the sensor chemistry to the desired analyte.

<u>Methods</u>

Materials: Peptoid synthesis, protein expression

All peptoid strands were synthesized and purified according to previously reported procedures[18]. β-Alanine tert-butyl ester was free-based from the HCl salt using 1 M aq. NaOH and extracted with DCM before preparation of 1 M solutions in DMF. All other amines were purchased from commercial suppliers

and used without further purification. Peptoids were prepared using a Rink amide resin (200 mg) from Protein Technologies with a loading of 0.64 mmol/g. Standard peptoid coupling proceeded in two steps, initial bromoacetylation with bromoacetic acid (0.8 M) and *N,N*-diisopropylcarbodiimide (DIC, 0.8 M) in *N,N*-dimethylformamide (DMF) for 2.5 minutes. Subsequent displacement with amine (1 M) in DMF lasted for 5 minutes. Chemical structures for all loopoids in this study are summarized in Table 1.

Shiga toxin 1 expression.

The gene for shiga toxin 1, subunit B (STX 1B) was cloned into a pMAL-c5x vector (New England Biosciences, Ipswich, MA) with a 6X histidine tag, flexible $(GGS)_4$ linker and tobacco etch virus (TEV) protease cleavage site directly upstream of the gene (no maltose binding protein tag from the vector was included). The plasmid was constructed *via* Gibson Assembly (Gibson Assembly® Master Mix, New England Biosciences, Ipswich, MA) of the linearized vector and the insert as a gene block with 20 base pair overlaps (custom gBlocks® Gene Fragments, Integrated DNA Technologies, Coralville, IA). The plasmid was transformed into chemically competent BL21 (DE3) *E. coli* (New England Biosciences, Ipswich, MA). For expression, 500 mL batches of Luria-Bertani (LB) medium were inoculated to 0.05 OD_{600} and allowed to grow to 0.6-0.8 OD_{600} at 37°C with shaking at 250 rpm. The temperature was then lowered to 30°C and over-expression was induced with 1 mM isopropyl β-D-1-thiogalactopyranoside (IPTG) for 3 hours. Cells were harvested by centrifugation and stored as pellets at -80°C until protein purification. Cells were re-dispersed in phosphate buffered saline pH 7.4 (PBS; 0.01 M phosphate buffer, 0.0027 M potassium chloride and 0.137 M sodium chloride) with 10 mM imidazole and lysed with an EmulsiFlex C3 homogenizer (Avestin Inc., Ottawa, ON, Canada). Insoluble cell debris was removed by centrifugation and the supernatant was applied to a 1 mL HisTrap™ Excel (GE Healthcare Life Sciences, Marlborough, MA) Ni-NTA column on an ÄKTA FPLC system (GE Healthcare Life Sciences, Marlborough, MA) equilibrated with PBS pH 7.4 with 10 mM imidazole. The column was washed with 40 mM imidazole and bound proteins were eluted with PBS pH 7.4 with 500 mM imidazole. The protein

was then dialyzed overnight into PBS pH 7.4 at 4 °C, the histidine tag was cleaved with TEV protease overnight at 4 °C, and the protein was then purified as a pentamer *via* gel filtration with a Superdex 200 Increase 10/300 GL column (GE Healthcare Life Sciences, Marlborough, MA). Samples were characterized by SDS-PAGE and Western blot (6X-His tag antibody-HRP conjugate; Invitrogen) concentrations were measured by UV-Vis spectroscopy, and samples were stored in PBS pH 7.4 at 4°C (Supplemental Figure S10).

Preparation of peptoid monolayer by Langmuir Blodgett technique.

The Langmuir trough (Mini-trough, KSV Nima, Finland) was filled with a subphase of 2 mM tris buffer (pH 8), equipped a paper Wilhelmy plate, and the surface was aspirated. A plasma-cleaned Si wafer with 300 nm of SiO_2 was next submerged in the subphase. Using a syringe 10 µL of 2 mM peptoid solution (1:1 water:DSMO) was spread on the interface. After spreading, 30 min was allowed for the monolayer to come to equilibrium. Once this was reached, the film was compressed at a rate of 10 cm^2/min until a pressure of 30 mN/m was obtained. After reaching this pressure the Si/SiO_2 wafer was pulled through the interface at a rate of 1 mm/min. During this process, the surface pressure was maintained at 30 mN/m, and the area of the trough decreased in direct correlation with the area of the wafer being pulled though the interface.

Preparation of peptoid bilayer by Langmuir Schaeffer technique.

Bilayer deposition was accomplished through the Langmuir-Schaeffer technique. First the monolayer was dried at 50 °C under vacuum for 2 hr to remove trapped water from between the film and the substrate and insure maximum adhesion of the monolayer to the substrate. A peptoid film was prepared on the Langmuir trough as described above with the exception of the substrate placement. In this case the substrate with a precoated monolayer is placed horizontally above the interface. Once the film is

compressed to 30 mN m^{-1} the substrate was lowered until it just touched the interface. At that point the interface was aspirated to remove the excess film and the substrate lifted until the subphase detached.

Fluorescence Microscopy

To image the bilayer films using fluorescence microscopy, they were first stained with Nile red. For this the substrates with the attached bilayer was submerged in 1 μm Nile red in water for 10 min. They were then removed and washed with pure water. After staining the films were imaged using 590 nm excitation.

AFM

Bilayer and monolayer films were directly imaged by AFM. Films were dried at 50 °C under vacuum for 2 hrs before imaging. AFM images were obtained on an Asylum MFP-3D AMF operated in tapping mode. Budget Sensors Tap150G probes were used for all imaging.

TEM

Monolayer and bilayer samples were prepared on a plasma etched continuous carbon TEM grid to allow for TEM analysis. The monolayer was deposited by pulling the grid through a compressed film as described above. The bilayer was produced by dropping the grid with the deposited monolayer onto a fresh film on the interface. The grid was then removed from the interface by placing a piece of paper over the grid on the interface and removing it. The grid attached to the paper and could be removed once the paper dried. The grid was washed 3x with pure water before analysis to insure any residual buffer was removed. Electron diffraction patterns were obtained with a Libra 200MC at the National Center for Electron Microscopy.

GIWAXS

Grazing incidence wide angle X-ray scattering data was collected at the Advanced Light Source beamline 7.3.3. For these experiments monolayers and bilayers were deposited on Si(111) using the methods described above. X-rays of 10 keV with and energy bandwidth of $E/\Delta E = 100$ were used. A Pilatus 2M detector from Dectris was used. Calibration of sample detector distance and beam center was performed with a silver behenate standard. The Nika package for IGOR pro was used to process the data.

Details of BLI sensing platform

BLI experiments were performed on an OctetRED96 BLI system (ForteBio, CA) using amine-coated optical sensors. Sensors were cleaned by immersion into 0.01 M sodium hydroxide solution for 1 hr. Then, 2-phenylethyl groups were functionalized on the surface of the glass sensors by the vaporization of 2-phenylethyltrichlorosilane during 2 hr. After the sensors were functionalized an annealed monolayer of the desired peptoid was deposited using the LS method. Before observation of protein binding, sensors were equilibrated for 20 min in PBS buffer containing 0.1% Tween 20. After reaching equilibrium state, sensors were moved into the solutions containing protein targets for obtaining association curve. Then, sensors were moved into PBS buffer for obtaining dissociation curve. Regeneration of sensor tips were carried out by using HCl treatment. Briefly, the surface of sensor tips were transferred into 10 mM HCl solution during 10 sec at room temperature for the removal of bound proteins. Then, sensors were neutralized during 10 sec in PBS buffer containing 0.1% Tween 20.

References

1.   A. K. Geim, K. S. Novoselov, The rise of graphene. *Nat Mater* **2007**, *6*, 183-191.

2.   The rise and rise of graphene. *Nat Nanotechnol* **2010**, *5*, 755.

3.   V. Müller, A. Hinaut, M. Moradi, M. Baljozovic, T. A. Jung, P. Shahgaldian, H. Möhwald, G. Hofer, M. Kröger, B. T. King, E. Meyer, T. Glatzel, A. D. Schlüter, A Two-Dimensional Polymer Synthesized at the Air/Water Interface. *Angew. Chem., Int*. Ed. **2018**, *57*, 10584-10588.

4.   J. Liu, W. Zan, K. Li, Y. Yang, F. Bu, Y.Xu, Solution Synthesis of Semiconducting Two-Dimensional Polymer via Trimerization of Carbonitrile. *J. Am. Chem. Soc*., **2017**, *139*, 11666-11669.

5.   R. Dong, T. Zhang, X. Feng, Interface-Assisted Synthesis of 2D Materials: Trend and Challenges. *Chem. Rev*. **2018**, *118*, 6189-6235.

6.   S. L. Cai, W. G. Zhang, R. N. Zuckermann, Z. T. Li, X. Zhao, Y. Liu, The Organic Flatland-Recent Advances in Synthetic 2D Organic Layers. *Adv. Mater.* **2015**, *27*, 5762.

7.   P. Mu, G. Zhou, C.-L. Chen, 2D nanomaterials assembled from sequence-defined molecules. *Nano-Structures & Nano-Objects* **2018**, *15*, 153-166.

8.   J. E. Murphy, T. Uno, J. D. Hamer, F. E. Cohen, V. Dwarki, R. N. Zuckermann, A combinatorial approach to the discovery of efficient cationic peptoid reagents for gene delivery. *Proc. Natl. Acad. Sci. U.S.A*. **1998**, *95*, 1517-1522.

9.   A. S. Knight, E. Y. Zhou, M. B. Francis, R. N Zuckermann, Sequence Programmable Peptoid Polymers for Diverse Materials Applications**.** *Adv. Mater*. **2015**, *38*, 5665–5691.

10. H. K. Murnen, A. M. Rosales, J. N. Jaworski, R. A. Segalman, R. N. Zuckermann Hierarchical Self-Assembly of a Biomimetic Diblock Copolypeptoid into Homochiral Superhelices. *J. Am. Chem. Soc*., **2010**, *132*, 16112-16119.

11. A. I. Nguyen, R. K. Spencer, C. L. Anderson, R. N. Zuckermann, A bio-inspired approach to ligand design: folding single-chain peptoids to chelate a multimetallic cluster. *Chem. Sci.* **2018**, *9*, 8806-8813.

12. X. Jiang, D. R Greer, J. Kundu, C. Ophus, A. M Minor, D. Prendergast, R. N. Zuckermann, N. P. Balsara, K. .H Downing. Imaging Unstained Synthetic Polymer Crystals and Defects on Atomic Length Scales Using Cryogenic Electron Microscopy**.** *Macromolecules* **2018,** *51*, 7794-7799.

13. K. T. Nam, S. A. Shelby, A. B. Marciel, P. C. Choi, R. Chen, L. Tan, T. K. Chu. R. A. Mesch, B. C. Lee, M. D. Connolly, C. Kisielowski, R. N. Zuckermann, Free-floating ultra-thin two-dimensional crystals from sequence-specific peptoid polymers *Nature Mater*. **2010**, *9*, 454-460.

14. J. Sun, X. Jiang, R. Lund, K. H. Downing, N. P. Balsara, R. N. Zuckermann, Crystalline polypeptoid nanotubes. *Proc. Natl. Acad. Sci.* **2016**, 113, 3954-3959

15. B. Sanii, R. Kudirka, A. Cho, N. Venkateswaran, G. K. Olivier, A. M. Olson, H. Tran, R. M. Harada, L. Tan, R. N. Zuckermann, Shaken, not stirred: Collapsing a peptoid monolayer to produce free-floating, stable nanosheets. *J. Am. Chem. Soc.* **2011**, *133*, 20808-20815.

16. E. J. Robertson, G. K. Olivier, M. L. Qian, C. Proulx, R. N. Zuckermann, G. L. Richmond, Assembly and molecular order of two-dimensional peptoid nanosheets through the oil–water interface. *Proc. Natl. Acad. Sci. USA* **2015**, *112*, 13284-13289.

17. B. C. Hudson, A. Battigelli, M. D. Connolly, J. Edison, R. K. Spencer, S. Whitelam, R. N. Zuckermann, A. K. Paravastu, Evidence for cis Amide Bonds in Peptoid Nanosheets. *J. Phys. Chem. Lett.* **2018**, 9, 2574-2578.

18. G. K. Olivier, A. Cho, B. Sanii, M. D. Connolly, H. Tran, R. N. Zuckermann, Antibody-Mimetic Peptoid Nanosheets for Molecular Recognition. *ACS Nano* **2013**, 7, 9276-9286.

19. E. J. Robertson, A. Battigelli, C. Proulx, R. V. Mannige, T. K Haxton, L. Yun, S. Whitelam, R. N. Zuckermann, Design, synthesis, assembly, and engineering of peptoid nanosheets. *Acc. Chem. Res.,* **2016,** *49*, 379-389.

20. C. Joy, W. Krista, W. Charles, C. Sae, Y. Danfeng, P. Henrik, W. Jing, L. Pu, H. Bettina, M. Weilei, V. Ram, Z. Lian-She, P. Donald, C. Greg, R. Michael, D. Kevin, H. Huddee, E. Tim, G. Juan, H. Michael, P.-W. Janette, L. Scott, Z. Robert, T. Hong, Label-Free Detection of Biomolecular Interactions Using BioLayer Interferometry for Kinetic Characterization. *Comb. Chem. High Throughput Screen.* **2009**, *12*, 791-800.

21. R. L. Petersen, Strategies Using Bio-Layer Interferometry Biosensor Technology for Vaccine Research and Development. *Biosensors* (Basel) **2017**, *7*, E49..

22. D. Yang, A. Singh, H. Wu, R. Kroe-Barrett, Comparison of biosensor platforms in the evaluation of high affinity antibody-antigen binding kinetics. *Anal. Biochem.* **2016**, *508*, 78-96.

23. L. Zhu, Z. Zhao, P. Cheng, Z. He, Z. Cheng, J. Peng, H. Wang, C. Wang, Y. Yang, Z. Hu, Antibody-Mimetic Peptoid Nanosheet for Label-Free Serum-Based Diagnosis of Alzheimer's Disease. *Adv. Mater.* **2017**, *29*, 1700057.

24. A. Battigelli, J. H. Kim, D. C. Dehigaspitiya, C. Proulx, E. J. Robertson, D. J. Murray, B. Rad, K. Kirshenbaum, R. N. Zuckermann, Glycosylated Peptoid Nanosheets as a Multivalent Scaffold for Protein Recognition *ACS Nano* **2018**, 12, 2455-2465.

25. B. Sanii, T.K. Haxton, G.K. Olivier, A. Cho, B. Barton, C. Proulx,; S. Whitelam, R. N. Zuckermann, Structure-Determining Step in the Hierarchical Assembly of Peptoid Nanosheets. *ACS Nano* **2014**, *8*, 11674-11684.

26. E.J. Robertson, E.M. Nehls, R.N. Zuckermann, Structure–Rheology Relationship in Nanosheet-Forming Peptoid Monolayers. *Langmuir* **2016**, *32*, 12146-12158.

27. D. Flood, C. Proulx, E.J. Robertson, A. Battigelli, S. Wang, A.M. Schwartzberg, R.N. Zuckermann, Improved chemical and mechanical stability of peptoid nanosheets by photo-crosslinking the hydrophobic core**.** *Chem. Commun.* **2016,** *52*, 4753-4756.

28. K. Gujraty, S. Sadacharan, M. Frost, V. Poon, R. S. Kane, J. Mogridge, Functional Characterization of Peptide-Based Anthrax Toxin Inhibitors. *Molecular Pharmaceutics* **2005**, *2*, 367-372.

29. M. Watanabe, K. Igai, K. Matsuoka, A. Miyagawa, T. Watanabe, R. Yanoshita, Y. Samejima, D. Terunuma, Y. Natori, K. Nishikawa, Structural Analysis of the Interaction between Shiga Toxin B Subunits and Linear Polymers Bearing Clustered Globotriose Residues. *Infection and Immunity* **2006**, *74*, 1984-1988.

30. P. M. St. Hilaire, M. K. Boyd, E. J. Toone, Interaction of the Shiga-like Toxin Type 1 B-Subunit with Its Carbohydrate Receptor. *Biochemistry* **1994**, *33*, 14452-14463.

31. M. Mourez, R. S. Kane, J. Mogridge, S. Metallo, P. Deschatelets, B. R. Sellman, G. M. Whitesides, R. J. Collier, Designing a polyvalent inhibitor of anthrax toxin. *Nat. Biotechnol.* **2001**, *19*, 958-961.

32.   M. Mammen, S.K. Choi, G.M. Whitesides, Polyvalent interactions in biological systems: implications for design and use of multivalent ligands and inhibitors. *Angew. Chem. Int. Ed. Engl.* **1998**, *37*, 2755-2794.

TOC graphic: